IOP Conf. Series: Materials Science and Engineering **406** (2018) 012009 doi:10.1088/1757-899X/406/1/012009

Effect of intra-ply voids on the homogenized behavior of a ply in multidirectional laminates

A Matveeva[1,*], D Garoz[2,3], R D B Sevenois[2,3], M Zhu[3,4], L Pyl[5], W Van Paepegem[2] and L Farkas[1]

[1] Siemens Industry Software NV, Interleuvenlaan 68, 3001, Leuven, Belgium
[2] Ghent University, Department of Materials, Textiles and Chemical Engineering – MaTCh, Tech Lane Ghent Science Park – Campus A, Technologiepark-Zwijnaarde 903, 9052 Zwijnaarde (Gent), Belgium
[3] SIM vzw, Technologiepark 935, 9052 Zwijnaarde (Gent), Belgium
[4] KU Leuven, Department of Materials Engineering, Kasteelpark Arenberg 44, 3001 Leuven, Belgium
[5] Department of Mechanics of Materials and Constructions (MeMC), Faculty of Engineering Sciences, Vrije Universiteit Brussel (VUB), Pleinlaan 2, 1050 Brussels, Belgium

* anna.matveeva@siemens.com

Abstract. This work focuses on the effect of intra-ply voids on the homogenized nonlinear behavior of a ply in multidirectional composites. Voids were modeled explicitly on the fiber scale and linked to the ply-scale by the recently developed two-scale framework which couples Classical Laminate Theory on the macro-scale with Finite Element analysis on the micro-scale. Laminates $[\pm 45]_{2s}$ and $[\pm 67.5]_{2s}$ were used as validation cases. The computed homogenized behavior of plies with and without voids for each laminate were compared against existing experimental data on manufactured plates. The nonlinearity of the homogenized stress-strain curves of all models is in a good agreement with experiments up to 1% of applied deformation for a laminate $[\pm 45]_{2s}$ and up to 0.4% for a laminate $[\pm 67.5]_{2s}$. The effect of voids was assessed only virtually and it is shown that 4% of void content decreases the ply strength by 30%, transversal Young's and shear moduli by around 10% and 8% respectively, whereas longitudinal stiffness is only slightly affected by the presence of voids. This work is the first step towards automatization of the virtual identification of the complete set of damage-plasticity parameters for the LMT-Cachan damage model accounting for the presence of intra-ply voids.

1. Introduction

The effect of voids on the mechanical behavior of the fiber reinforced composites, including multidirectional laminates and textile based composites attracts attention of the composite community since many years. A recent review of the effect of voids on the mechanical properties of composites can be found in [1]. One of the main conclusions is that, despite the extensive amount of available research, further assessment of the effect of voids is needed. This especially in automotive and aerospace industry, where voids are the key defects in manufacturing techniques such as out-of-autoclave (OoA) and automated tape laying (ATL).

In [2] a multiscale approach to account for effect of voids is presented. The local material properties including transverse strength and Mode I fracture toughness are computed in the presence of voids at the scale of fibers (micro-scale) and then subsequently homogenized to the ply-scale (macro-scale) and

assigned to "weak volumes", representing the presence of voids. Extended Finite Element (XFEM) is employed at the ply-scale to analyze the crack density evolution in cross-ply laminates with and without the presence of voids. This approach allows to track initiation and propagation of multiple cracks in a ply, as well as to link them to inter-laminar cracks/delamination [3]. The alternative to the time-consuming simulations with XFEM, is to use Continuum Damage Models (CDM) at the ply-scale, where the properties of the ply/or the region of interest are degraded based on a damage evolution law, which can be modified according to the void content at the lower scale.

A ply damage model developed at LMT-Cachan [4–6] and implemented in the FE code Siemens PLM Software LMS Samtech SAMCEF [7] couples the damage evolution in the transverse and in-plane shear directions taking into account the plastic behavior of the reinforced polymer. It is also possible to address the damage evolution in the fiber direction and through-the-thickness. The model has been validated for intra-laminar behavior at the coupon level for UD plies [8]. The model requires several input parameters characterizing elastic behavior, damage, plasticity and final ply failure. The parameter identification requires experimental tests on different laminates, such as quasi-static tensile and compression tests on $[0/90]_{4s}$ laminates and cyclic tensile tests on $[\pm45]_{2s}$ and $[\pm67.5]_{2s}$ laminates [4, 8, 9]. The effect of voids on the composite mechanical properties and on the set of parameters for LMT-Cachan model has been investigated in [10]. A clear influence of voids on the damage initiation and propagation and hence on the parameters of the LMT-Cachan damage model was established. Such experimental assessments of the effect of voids is very challenging, especially if to compare the effect against the reference material without voids. By changing the manufacturing parameters, e.g. by lowering the autoclave pressure and the cure temperature, and ensuring the presence of voids in a composite, the behavior of its constituents, mainly the matrix and the fiber/matrix interface might be affected [11]. To decouple the influence of voids from the influence of manufacturing parameters is not a straightforward task. Instead, a virtual parameter identification can offer a promising alternative, however the validation of the methodology is challenging for the same reasons. In [12] Garoz et al. provides a methodology to identify parameters of the LMT-Cachan damage model by means of dedicated micro-mechanical virtual tests with detailed constituent material models, representative geometry and specific load conditions. In order to verify the approach, Garoz et al. compared the ply model with the identified parameters (based on physical tests) against the micro-mechanical virtual tests on the $[\pm45]_{2s}$ and $[\pm67.5]_{2s}$ laminates. The two approaches gave the same results, except for some small discrepancies in the transverse stress-strain curve of the virtual test on the $[\pm67.5]_{2s}$ laminate. In the current study, the proposed workflow in [12] was further modified by considering the presence of voids at the micro-scale level.
To assess the methodology, firstly, micro-mechanical virtual tests on a void-free material were employed with the objective to compare the homogenized behavior of plies in $[\pm45]_{2s}$ and $[\pm67.5]_{2s}$ laminates under the static tensile loading against existing experimental data on the laminates. Secondly, voids were embedded at the micro-scale and their effect on the homogenized ply behavior was virtually assessed.

2. Material and Experiments

The composite laminates used in this work are manufactured from unidirectional (UD) prepregs PYROFIL™ TR 360E250S supplied by Honda R&D Co., Ltd. and Mitsubishi Chemical Corporation [13]. The prepregs were made of polyacrylonitrile (PAN) based carbon fibers embedded in PYROFIL #360 resin with a volume fraction of 60%. Several plates were made of UD prepregs with a stacking sequence $[0]_4$, $[90]_8$, $[\pm45]_{2s}$, $[\pm67.5]_{2s}$. The plates were tested under static tension and measured stress-strain curves served as reference data for modelling results. Several tests on constituents were performed to obtain the input data for the models.

2.1. Input data for the micro-scale model

- Fiber properties

The elastic properties of the carbon fiber are reversed engineered from the 3D homogenized elastic tensor of the UD ply [14]. Full 3D orthotropic elastic stiffness tensor of the ply is computed by measuring

the propagation velocity of both the longitudinally and transversally polarized bulk waves at various symmetry planes of a UD Carbon/Epoxy laminate using ultrasonic insonification. Determined Young's moduli, shear moduli and Poisson's ratios can be found in table 1. For the in-depth discussion on the effect of high frequencies produced by the ultrasound on the elastic properties of the material under investigation, the reader is referred to [14].

- Matrix behavior in tension

To test the matrix behavior in tension, static tensile tests on the matrix were performed according to the ASTM D638 using a testing machine Instron 5567 with mechanical wedge-type clamps and the test speed 2 mm/min. The tests were accompanied by a mechanical extensometer and a Digital Image Correlation (DIC) Limess VIC 3D system, in 2D mode with one camera. 5 samples were tested, all failing in the gauge section with a brittle failure. The moduli of elasticity were calculated as a slope of the stress-strain curves between 0.1% and 0.3% strain. Table 1 contains average values and standard deviations of Young's modulus and maximum strain at failure in tension, measured by DIC.

- Matrix behavior in shear

To test the matrix behavior in shear, static tensile tests on the matrix were performed according to the ASTM D5379 using a testing machine Instron 5800R with Iosipescu test setup and the test speed 1 mm/min. The tests were accompanied by a DIC system: VIC 3D system, 3D mode with two cameras. The shear modulus was calculated as a maximum progressive slope of the longitudinal stress-strain curve using DIC. Table 1 contains average values and standard deviation of shear modulus measured by DIC.

- Interface

The properties of the interface were not measured for this set of fibers and the matrix. Interfacial strength and toughness are taken from [15] for a similar carbon/epoxy material.

Material properties of the constituents are summarized in table 1.

Table 1. Material properties of constituents

Fibers [14]	
Property	**Value**
Young's moduli	
E_{11} (GPa)	23.3
E_{22} (GPa)	18.4
E_{33} (GPa)	18.4
Poisson's ratio	
ν_{12}(-)	0.02
ν_{13}(-)	0.02
ν_{23}(-)	0.27
Shear moduli	
G_{12} (GPa)	36.9
G_{13} (GPa)	36.9
G_{23} (GPa)	7.2
Fiber radius	
r (μm)	3.6

Matrix	
Property	**Average value (std)**
Young's modulus	
E (MPa)	2.84 (0.1)
Shear modulus	
G (MPa)	0.97 (0.013)
Poisson's ratio	
ν (-)	0.46[a]
Strain at failure in tension	
ε_f^t (%)	2.63 (0.01)
Strain at failure in shear	
γ_f^s (%)	11 (0.03)

Interface [15]	
Property	**Value**
Interface maximum strength	
τ_n (MPa)	50
τ_t (MPa)	75
Interface critical strain energy release rates	
G_{IC} (N/mm)	0.002
G_{IIC}, G_{IIIC} (N/mm)	0.006
Mixed-mode interaction parameter	
η (–)	1.45

[a] *matrix Poisson's ratio was calculated to fulfil the isotropic assumption of G=E/(2(1+ν))*

2.2. Data used for validation of the macro-scale behavior

- UD laminate

Several plates made of 4-ply UD prepregs with a stacking sequence $[0]_4$ and $[90]_8$ were tested under tension to derive longitudinal and transverse Young's moduli of a ply. A testing machine Instron 4505 with mechanical wedge-type clamps and the test speed 2 mm/min was equipped with Instron extensometer and digital image correlation (DIC system): Limess VIC 3D system, 3D mode with two cameras. Transverse modulus in table 2 was calculated from results on $[90]_8$ laminate as a slope of the stress-strain curve using DIC between 0.05% and 0.1% strain. Longitudinal modulus in table 2 was calculated from results on $[0]_4$ laminate as a slope of the stress-strain curve using DIC between 0.1% and 0.3% strain. DIC Poisson's ration was calculated using DIC response in linear stress-strain curve from the results on $[0]_4$ laminate based on longitudinal and transverse strain available from DIC measurements.

- Laminates $[\pm45]_{2s}$ and $[\pm67.5]_{2s}$

Produced laminates with a stacking sequence $[\pm45]_{2s}$ and $[\pm67.5]_{2s}$ were tested according to ASTM D3039. Laminates $[\pm67.5]_{2s}$ were tested in different loading phases, instead of immediate test to failure. A testing machine Instron 4505 with mechanical wedge-type clamps and the test speed 2 mm/min was equipped with Instron extensometer and digital image correlation (DIC system): VIC 3D system, 3D mode with two cameras. Shear modulus in table 2 was calculated from results on $[\pm45]_{2s}$ laminate as a slope of the shear stress-strain curve using DIC between 0.2% and 0.6% strain. Measured stress-strain curves are presented in the result section (figure 6, figure 7, figure 8) in a local coordinate system (CS) of a ply, the transformation was done as proposed in [4].

Table 2. Material properties of a UD ply

UD (ASTM + DIC)	
Property	Average value (std)
Young's moduli	
E_{11} (GPa)	127.52 (1.24)
E_{22} (GPa)	8.49 (0.721)
Poisson's ratio	
ν_{12}(-)	0.34 (0.0143)
In-plane shear modulus	
G_{12} (GPa)	4.11 (0.23)
Maximum shear stress	
$\tau_{12}^{\max}$ (MPa)	52.27 (0.95)
Maximum shear strain	
$\gamma_{12}^{\max}$ (%)	3.66 (0.96)

3. Virtual Material Characterization with the VMC ToolKit

The Simcenter™ VMC ToolKit of Siemens PLM Software is a set of software tools developed for virtual material characterization (VMC) to replace physical tests with virtual experiments. The VMC ToolKit allows detailed material modelling at different scales and covers wide range of supported composite types, such as UD plies, 2D/3D woven, non-crimp, weft-knitted, 2D/3D braided fabrics. More detailed concept of the tool can be found in [16]. Several validation cases to predict elastic properties of different composites are demonstrated in [17–19]. Current results are based on the recent extension of the VMC ToolKit towards prediction of non-linear and damage behavior accounting for the presence of voids at the fiber scale.

3.1. Micro-scale FE models with the presence of voids

To estimate the "as-manufactured" properties of specimens, *Random Packing* (RP) functionality of the VMC ToolKit was extended with a feature of *Void Generation* at the fiber scale. The matrix is modeled as a solid body with voids of different shapes (cylindrical and spheroidal) and different sizes. The percentage of voids in the model and their spatial distribution can vary according to user input. UD fibers remain to have constant diameters and random distribution in the matrix with predefined volume fraction. The algorithm [20] was employed to randomly distribute fibers in the matrix with a modification of randomizing the minimum distance between fibers [21]. Fibers and cylindrical voids are generated as an extrusion of corresponding circular cross sections through the unit cell thickness and spheroidal voids are revolved according to their equatorial radius (minor radius) and the distance from the center to pole along the symmetry axis (major radius). Radii of voids, as well as a through-the-thickness position of spheroidal voids can be defined either randomly or manually as a user input.

Three different test cases of periodic unit cells of randomly distributed fibers in a matrix are generated: matrix being modelled without voids, matrix containing spheroidal voids with void fraction of 2.3% and matrix containing spheroidal voids and cylindrical voids with void fractions of 2.2% and 1.9% respectively (see figure 1). The cylindrical void was placed in the center of the unit cell with a radius of 3 microns. The size of spheroidal voids was randomly chosen between 1 and 3 microns for both minor and major radii. The dimension of the voids and their volume fractions were chosen randomly from the range of values found in literature [1]. In all cases the size of the unit cell is 38.5 x 38.5 x 3.85 μm^3, the radius of the fibers is 3.6 μm and the fiber volume fraction is fixed to 60%.

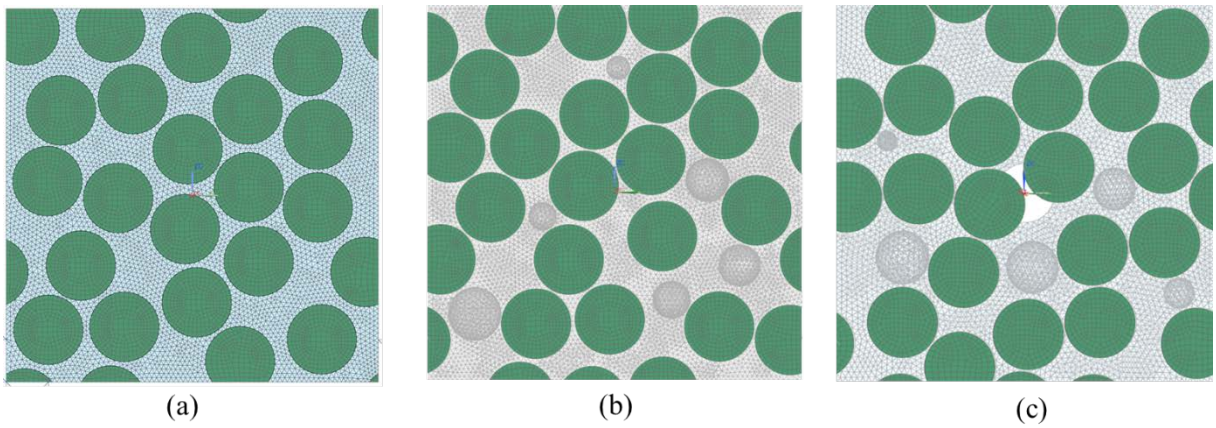

Figure 1. (a) RP model without voids; (b) RP model with 2.3% of spheroidal voids; (c) RP model with 2.2% of spheroidal voids and 1.9% of cylindrical voids.

In all three models, the matrix is discretized using linear 4-node tetrahedal solid elements and fibers using the 8-node hexagonal solid elements, both with an average element size of 0.5 micron. The interface between fibers and the matrix is modeled by cohesive elements: zero-thickness 8-node hexagonal cohesive elements automatically generated. Discretization of the unit cells with second order elements and further mesh-sensitivity analysis is under investigation.

3.2. The applied material behavior's

The fibers were modeled by transversely isotropic material without damage with elastic properties summarized in table 1. The behavior of the matrix is modeled with elasto-plastic constitutive model (properties listed in table 1). The plastic behavior of the matrix is described with Raghava yield criteria and tabulated engineering stress-strain curve for tension. The ratio between compression and traction limit for Raghava yield criteria is fixed to a default value of 1.3 due to absence of the test data in compression. The damage model for the matrix is an isotropic material model with damage. Once the

equivalent plastic strain has reached the limit, a static damage, d^s, is put to 1 and the true damage is obtained by solving the following law, expressing the damage rate:

$\dot{d} = \frac{1}{\tau_c}(1 - \exp(-a_c\langle d^s - d\rangle_+))$, τ_c and a_c are parameters for the delay law, set to 0.001 and 1 without any physical relevance, used for solver stability. The elastic Hooke tensor is degraded by scaling with *(1-d).* The equivalent plastic strain at failure was obtained by comparing the stress-strain curves on a single element patch test of a pure matrix against experimental data.Considering that the main deformation mechanism of the laminates under consideration is shear, equivalent plastic strain at failure was obtained by calibrating the material data in terms of shear strain to failure. Dotted curves (figure 2) are the updated laws of available test data in shear and in tension, obtained by loading a single element model of pure epoxy in tension and in shear with periodic boundary conditions. The extension of the stress-strain curves introduces artificial behavior in the unit cell, allowing the unit cell to deform much more in tension than in reality and therefore to reach higher stresses. To overcome this limitation, an application of a different plasticity-damage model for the matrix to be considered. In the Section 4 it will be shown, that the strain at failure of the matrix set to 11% led to a significant difference in strength of the ply against the experimental curve. One of the possible explanations is that at the micro-scale matrix should be capable to bare larger deformations before the failure. In [22], a matrix tested at the micro-scale shows a much-higher strain to failure than in conventional mechanical setups. Therefore an assumed and increased value of strain to failure up to 58% was also considered in this work. This value comes from a different epoxy matrix [19].

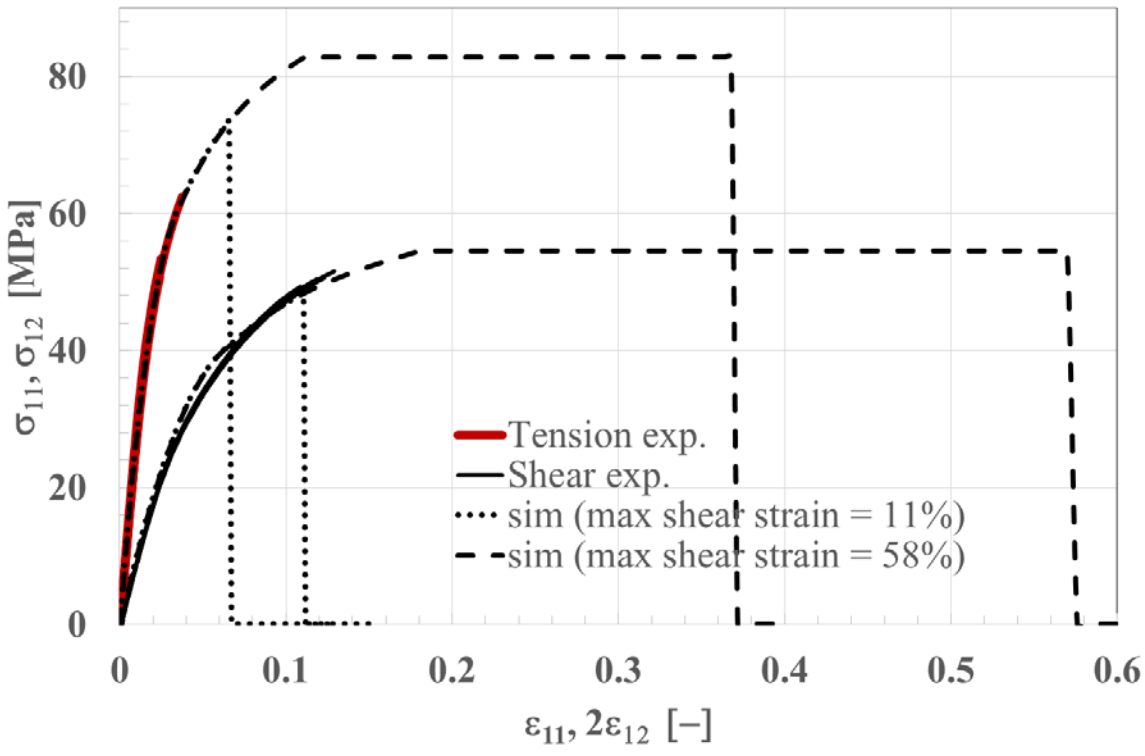

Figure 2. Strain-stress behavior of the epoxy matrix in experiments and simulations for tension and shear

The interface between fibers and the matrix is modelled with a damage interface material model called cohesive zone model. The cohesive behavior is governed by a damage initiation criterion and a damage evolution criterion, both are energy-based formulations. The bi-triangular cohesive parameters are listed in table 3, which are based on the experimental data presented in table 1. The elastic interfacial

characteristics are chosen by trial-and-error: they should be rather high to model continuity and not too high to avoid numerical divergence.

Table 3. Input data for the interface material model

Property	**Units**	**Value**
Transverse Stiffness (K03)	N/mm^3	2e+07
Shear Stiffness (K02 and K01)	N/mm^3	1.5e+07
Critical strain energy release rates (GIc, GIIc, GIIIc)	N/mm	0.002 0.006 0.006
Energy Threshold (Y0S)	N/mm	6.25e-05
Coupling Coefficient (DCOU)	-	1.45
Law Option		Bi-triangular
Time for Delay (TAU)	s.	0.001

3.3. Loading for linear and nonlinear homogenization

In order to compute linear-elastic properties of a ply, six load cases are applied on the generated micro-scale unit cells: three in tension and three in shear under periodic boundary conditions. The process works also on non-symmetrical meshes, which becomes valuable on complex models [23, 24]. The loading of a unit cell is done by imposing mean strains on a special *Homogenization* element implemented in SAMCEF and dedicated to perform homogenization of a unit cell. To assess material variability in terms of fiber and void distribution, ten configurations for each test case were generated. The average linear-elastic properties and standard deviations are computed and compared with available experimental data.

In [12], Garoz et al. developed a process for micro-mechanical tests capturing the damage mechanisms at the micro-scale and specific load conditions coupled with the Classical Laminate Theory (CLT) on the laminate scale. The concept is implemented to determine the initiation and propagation of the cracks in the ply and to mimic the virtual tests on multidirectional laminates. The current implementation is limited to laminates with $[\pm 45]_{2s}$ and $[\pm 67.5]_{2s}$ stacking sequences. This is linked to the identification of damage-plasticity material parameters for the LMT-Cachan damage model covering transverse and shear material behavior.

First the CLT is utilized to obtain a link between applied deformations of a laminate in longitudinal direction and local strain field in each ply in their local coordinate systems. Secondly, the ply is modeled as a unit cell with randomly distributed fibers in a matrix, as described in the section 3.1 and 3.2, and loaded with pre-calculated strains equivalent to the macro-strain loading. The load conditions are introduced using three dummy nodes per direction x; y; z. Each simulation provides stress-strain fields, from where homogenized stress-strain curves are derived. GUI for the stiffness and damage homogenization pre-processing steps are shown in Figure 3.

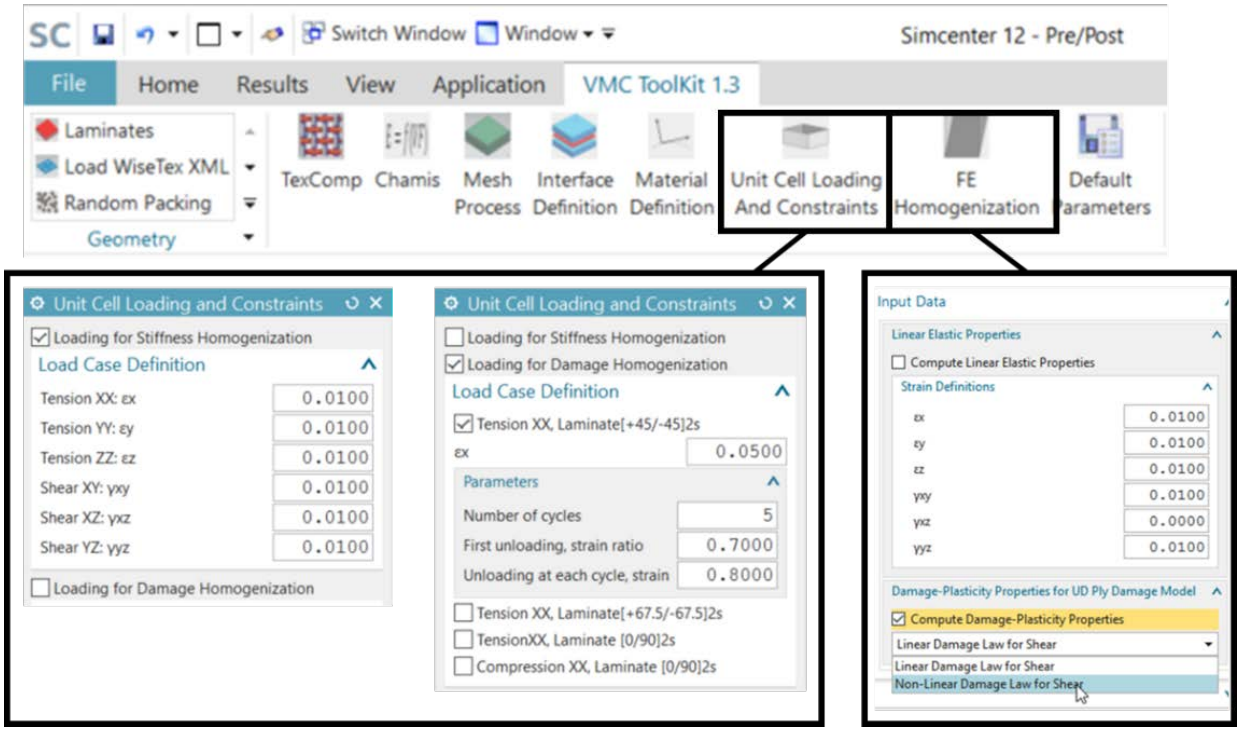

Figure 3 Graphical User Interface of the VMC ToolKit: *Unit Cell Loading and Constraints* and *FE Homogenization*

4. Results and discussion

4.1. Effect of voids on the linear elastic properties

The results on the linear elastic properties are summarized in figure 5. Longitudinal Young's modulus shows a difference of 6.5% between numerical data and experimental measurements. The effect of voids on the longitudinal Young's modulus is negligible. Longitudinal shear moduli display 9% difference between the 0.0%-void simulation and experimental results. The model with a void content of 4.1% shows a decrease in longitudinal in-plane shear modulus by 1.7 % and in longitudinal out-of-plane shear modulus by 3.0% in comparison with the 0.0%-void model. The difference between in-plane and out-of-plane longitudinal shear moduli can be eliminated by increasing number of fibers in the unit cells or by increasing number of tested configurations for each test case.

Values for transverse Young's moduli in the 0.0%-void model are higher than the experimental results by 14%. For transverse shear moduli, the experimental data is not available. Both, transverse Young's moduli and transverse shear moduli appear to decrease with void content by 10.0% and 7.86%, respectively.

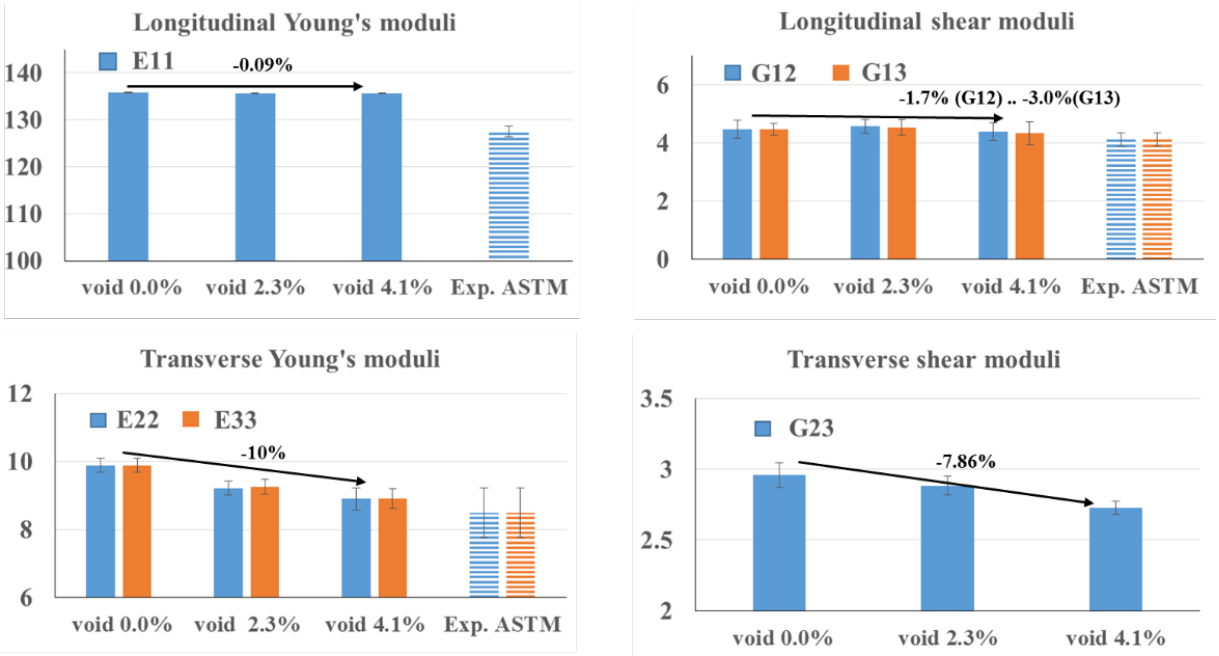

Figure 4. Effect of voids on linear elastic properties of a UD ply

4.2. Effect of voids on the nonlinear behavior of a ply

Figure 6 contains in-plane shear stress-strain curve of a [-45] ply in a laminate $[\pm 45]_{2s}$ when the shear strain at failure of the matrix was set to 11%. A significant difference in the maximum stress is observed in comparison with experimental results. The same figure demonstrates the damage development at different values of macro-strain of the model containing 4.1% of both cylindrical and spheroidal voids. Damage in the matrix started in few locations (point 1), joining in one crack (point 2) but not at the cylindrical void, where the highest stress concentrations are expected. The complete failure occurred at around 1.3% of applied shear deformations (point 3) driven only by the damage in the matrix and only a few debondings were observed. The maximum stress in the void-free model is 25% higher than in the model containing 4.1% voids.

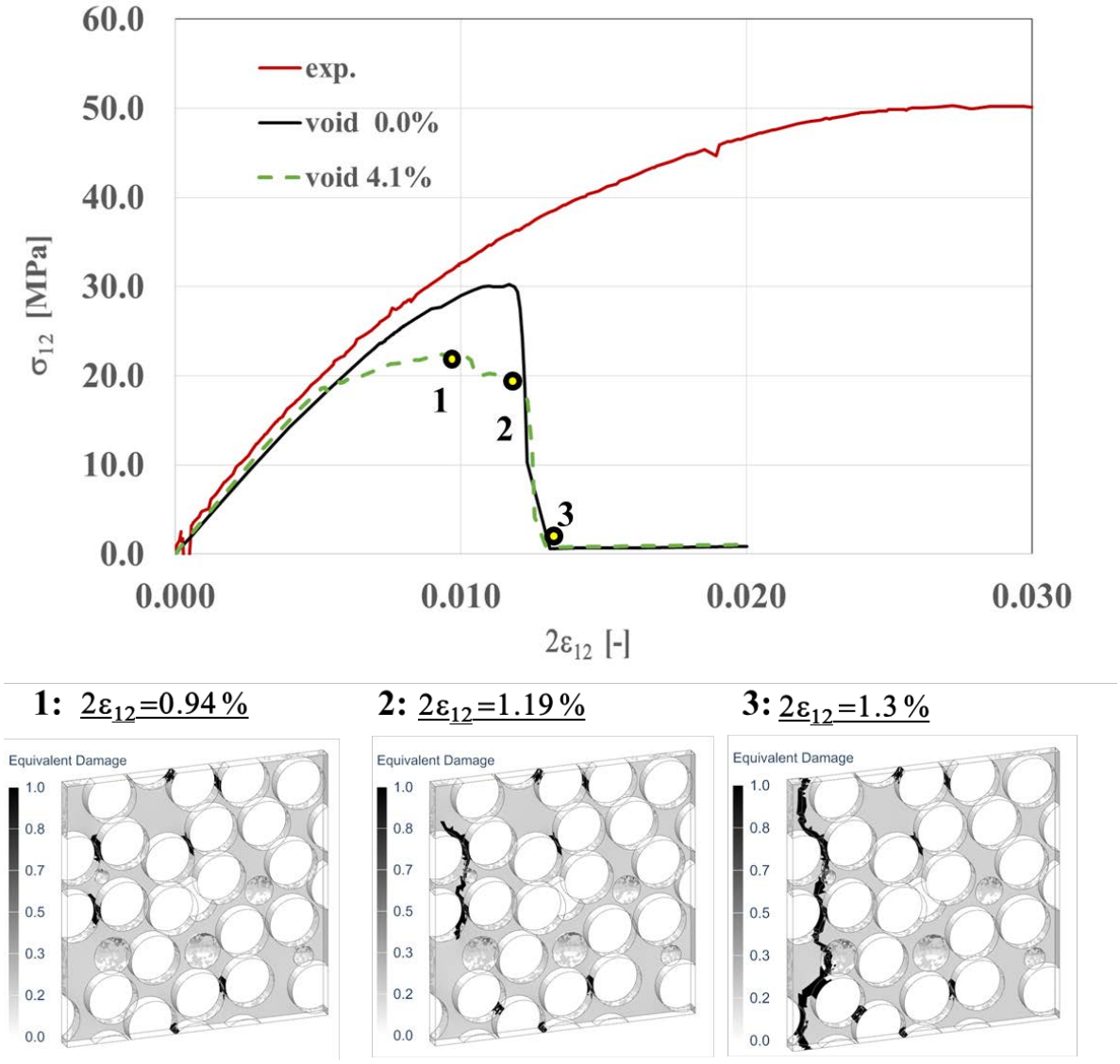

Figure 5. Homogenized stress-strain curves in shear direction in [-45] ply from the virtual test on the $[\pm 45]_{2s}$ laminate (shear strain at failure of the matrix was set to 11%) and damage development in the model containing 4.1% voids

One of the possible reasons that the models with strain to failure of 11% fail so early is because the cracks are restricted by the neighbouring plies only within the linear CLT allowing cracks to progress freely through the structure and causing early failure. Further investigation of this phenomena is needed. Another reason for the discrepancy with the experimental results, as was mentioned earlier (Section 3.1), is that the deformations of the matrix at the micro-scale up to failure can be higher than 11% (scale-effect). To analyze the effect of strain to failure of the matrix on the homogenized behavior of a ply, the computations are repeated with a strain at failure in a matrix of 58% presented in figure 7. Point 1 corresponds to the formation of few fiber/matrix debondings at the locations of highest stress concentrations. With increased applied deformation, debonds are starting to merge into a single debond in the vicinity of the cylindrical void (point 2). Further increased applied deformation results in the continuation of the debond growth with a formation of cracks in the matrix, bridging debonds (point 3). The maximum stress value of the model with voids is 30% higher than in the model without voids. The difference in shear strength between models with 0%, 2.3% and 4.1% of void content and experimentally measured strength is 11.7 %, -9.2 % and -20.7 % respectively.

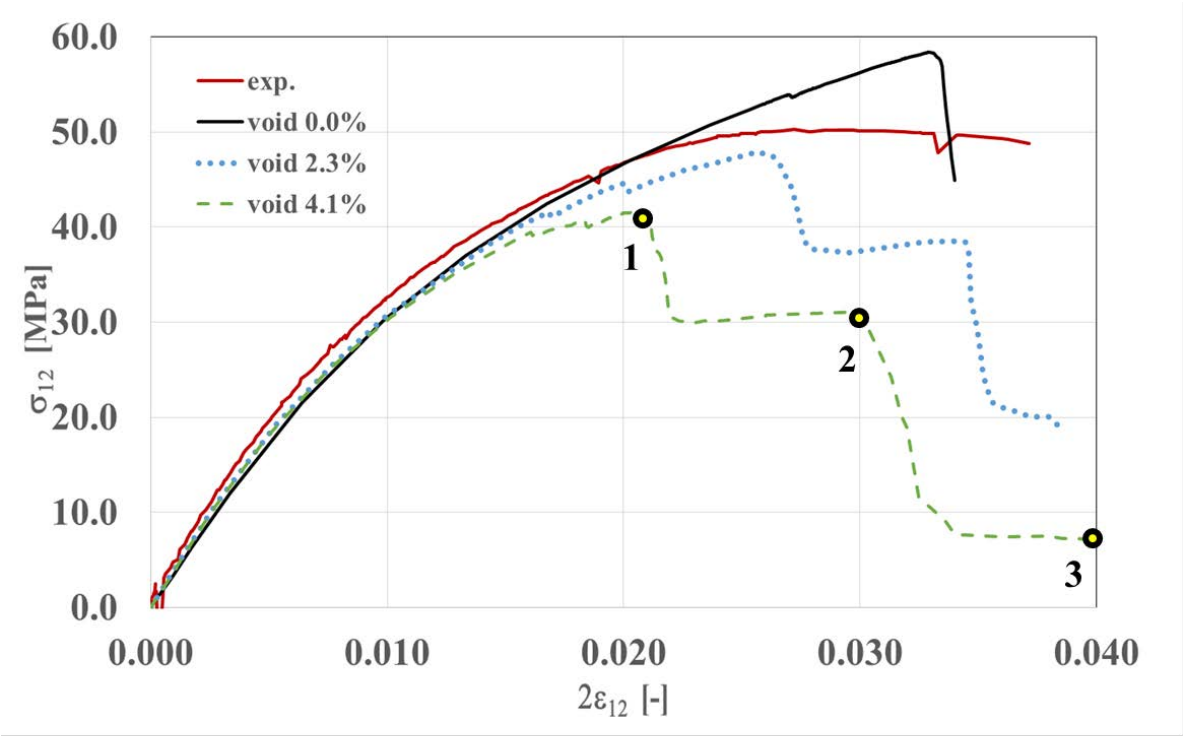

Figure 6. Homogenized stress-strain curves in shear direction in [-45] ply from the virtual test on the $[\pm 45]_{2s}$ laminate (shear strain at failure of the matrix was set to 58%) and damage development in the model containing 4.1% voids

Figure 8 presents results of virtual testing on laminates $[\pm 67.5]_{2s}$. Homogenized stress-strain curves in shear and in transverse direction are compared between all three cases and experimental data. The difference in shear strength between models with 0%, 2.3% and 4.1% of void content and experimentally measured strength is 2.6%, 7.6% and -5.4% respectively. The difference in transverse strength between models with 0%, 2.3% and 4.1% of void content and experimentally measured strength is 19%, 9.2% and -11.8% respectively.

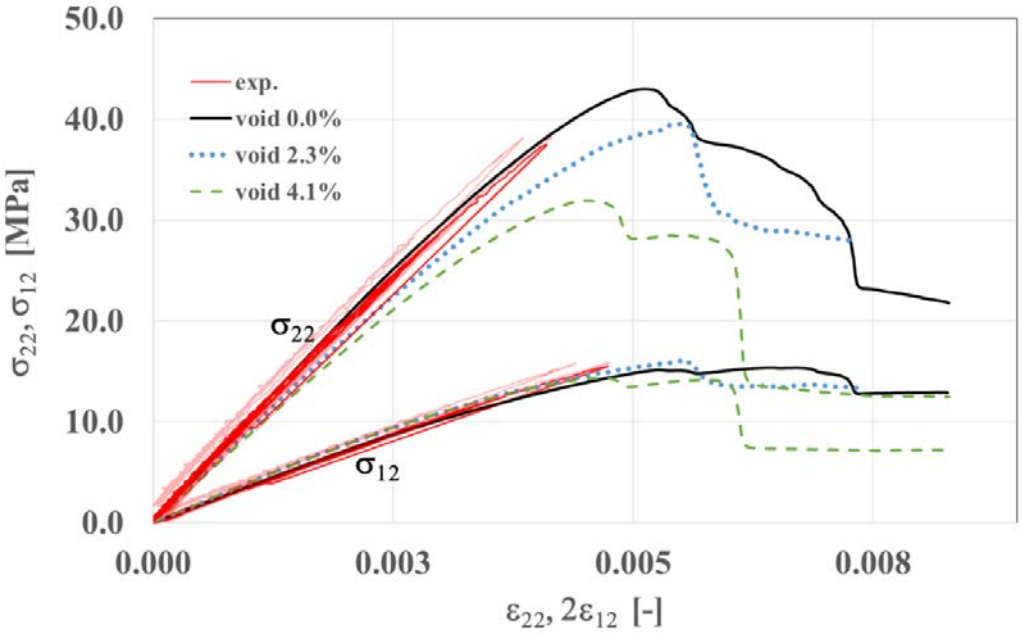

Figure 7. Homogenized stress-strain curves in shear and transverse direction in [-67.5] ply from the virtual test on the $[\pm 67.5]_{2s}$ laminate (shear strain at failure of the matrix was set to 11%).

The summary of maximum ply stresses is presented in figure 9. The decrease of strength between the void-free model and model with 4.1 % voids is 30% in shear directions for laminate $[\pm 45]_{2s}$ and 25% for laminate $[\pm 67.5]_{2s.}$ in transverse direction. The effect of voids on the maximum stresses in shear direction for laminate $[\pm 67.5]_{2s}$ is less pronounced and equals to 7%. Important to note that periodic boundary conditions are currently applied on the micro-scale models, which results in a periodic repetition of the damage across the ply. Therefore, strength values presented here should not be treated as absolute values, because the ply cracking considering crack evolution would affect the predicted material behavior.

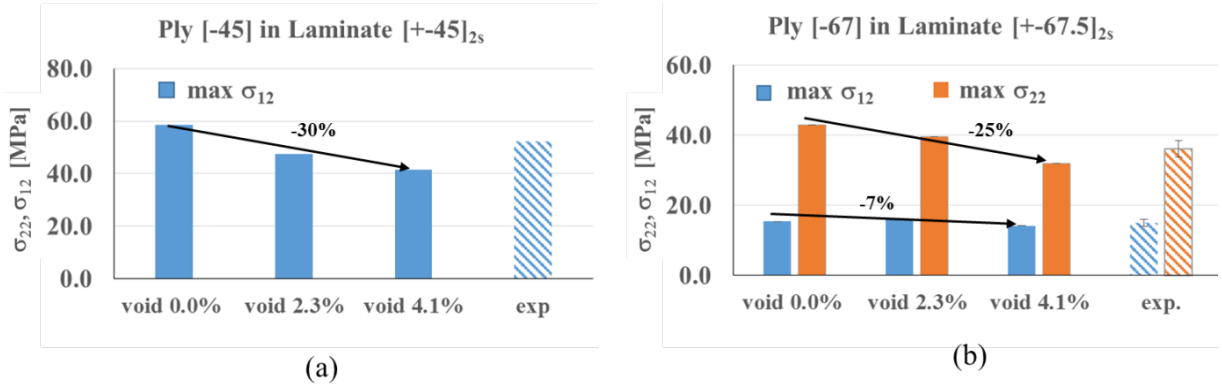

Figure 8. Effect of voids on maximum shear and transverse stress in a UD ply: (a) in ply [-45] from the virtual test on the $[\pm 45]_{2s}$ laminate; (a) in [-67.5] ply from the virtual test on the $[\pm 67.5]_{2s}$ laminate

5. Conclusions and future work

To estimate the "as-manufactured" properties of specimens, the Simcenter™ VMC ToolKit was extended with a feature of void generation at the fiber scale together with a special set of loadings and homogenization in order to perform virtual testing on multidirectional laminates. Simulations on the laminates $[\pm 45]_{2s}$ and $[\pm 67.5]_{2s}$ are conducted with and without voids, that are explicitly modeled at the fiber scale with different void type and content. In order to achieve this, several unit cells were generated and loaded with a complex equivalent macro-strain fields, which are computed from deformations of a ply using CLT.

First, the effect of voids was assessed on the linear elastic properties of the ply. For this, three tensile and three shear load cases were performed in order to build the full stiffness tensor and to compute linear elastic constants. It is shown that the presence of voids does not affect much the longitudinal elastic properties, and decreases the transversal Young's and shear moduli by around 10% and 8% respectively (for a void content of 4.1%). The effect of voids was as well analyzed on the strength/damage behavior of the ply. The nonlinearity of the homogenized stress-strain curves of all models is in a good agreement with experiments up to 2% of shear macro-strain for a laminate $[\pm 45]_{2s}$ and up to 0.4% for a laminate $[\pm 67.5]_{2s}$. The introduction of 4.1% of voids led to a decrease of maximum shear stresses in a laminate $[\pm 45]_{2s}$ of approximately 30%. The effect of voids in the laminate $[\pm 67.5]_{2s}$ is showing the decrease of transverse strength in a ply by 25% and the decrease of shear strength in a ply by 8%. Due to a limitation of the methodology with respect to a crack evolution through the laminate, these values rather indicate a possible trends on the effect of voids on the material failure. This paper is a demonstrator of a virtual material characterization process based on an engineering workflow implemented in Simcenter™ VMC ToolKit that predicts the macro-scale effect of key micro-scale material features, facilitating efficient material performance assessment in a bottom-up approach or facilitating virtual material optimization in a top-down approach.

Acknowledgments

The authors gratefully acknowledge SIM (Strategic Initiative Materials in Flanders) and VLAIO (the Agency Flanders Innovation & Entrepreneurship) for their support of the IBO project M3Strength (Grant no.140158), which is part of the research program MacroModelMat (M3), coordinated by Siemens (Siemens PLM Software, Belgium). The authors express their gratitude towards Honda R&D Co., Ltd., and Mitsubishi Chemical Corporation for their generosity in supplying material for this research.

References

[1] Mehdikhani M, Gorbatikh L, Verpoest I and Lomov S V 2018 Voids in fiber-reinforced polymer composites: a review on their formation, characteristics, and effects on mechanical performance *J. Compos. Mater. In print*

[2] Mehdikhani M, Petrov N A, Straumit I, Melro A R, Lomov S V and Gorbatikh L 2018 The effect of voids on matrix cracking in composite laminates revealed through combined modeling at the micro- and meso-scales *In preparation*

[3] Petrov N A, Gorbatikh L and Lomov S V 2017 A parametric study assessing performance of eXtended Finite Element Method in application to the cracking process in cross-ply composite laminates, *Composite Structures.* **187**, 489-497

[4] Ladevèze L and LeDantec E 1992 Damage modelling of the elementary ply for laminated composites," *Composites science and technology*, **43**(3), 257–267

[5] Ladevèze P 1992 A damage computational method for composite structures, *Computers and Structures*, **44**, 79–87

[6] Ladevèze P, Allix O, Gornet L, Lévêque D and Perret L 1998 A computational damage mechanics approach for laminates: Identification and comparison with experimental results, *Damage Mechanics in Engineering Materials*, 481–500

[7] Delsemme J P, Bruyneel M, Jetteur P, Magneville B, Naito T and Urushiyama Y 2015 Progressive damage modeling in composites: from aerospace to automotive industry, *Proc* in

Third Int. conf. on Buckling and Post-buckling Behavior of Composite Laminated Shell Structures, p 22-26, Braunschweig, Germany
[8] Bruyneel M, Delsemme J, Goupil A, Jetteur P, Lequesne C, Naito T and Urushiyama Y 2014 Damage modeling of laminated composites: validation of the intra-laminar law of SAMCEF at the coupon level for UD plies," in *Proc of the 16th European conf. on composite materials*, Seville, Spain
[9] Malgioglio F, Carella-Payan D, Magneville B and Farkas L 2016 Parameter Identification for interlaminar damage modelling of composites, *In Proc of the 6th ECCOMAS Thematic Conf. on the Mech. Response of Composites,* Eindhoven, Netherlands
[10] Steensels E 2017 Mechanical damage in carbon fibre-reinforced composites: experimental observations and model validation, *Maser Thesis, K.U. Leuven*
[11] Mehdikhani M, Standaert A, Steensels E, Vallons K, Gorbatikh L and Lomov S. V 2018 Multi-scale digital image correlation for detection and quantification of matrix cracks in carbon fiber composite laminates in the absence and presence of voids, *Compos. Part B-eng. under review*.
[12] Garoz D, Gilabert F A, Sevenois R D B, Spronk S W F and Van Paepegem W 2017 Material parameter identification of the elementary ply damage mesomodel using virtual micro-mechanical tests of a carbon fiber epoxy system, *Composite Structures*, **181**, 391–404
[13] Mitsubishi Chemical Corporation, https://www.m-chemical.co.jp/en/index.html
[14] Sevenois R D B, Garoz D, Verboven E, Spronk S W F, Gilabert F A, Kersemans M, Pyl L and Van Paepegem W 2018 Multiscale Approach for Identification of Transverse Isotropic Carbon Fibre Properties and Prediction of Woven Elastic Properties using Ultrasonic Identification, *under review*
[15] Arteiro A, Catalanotti G, Melro A, Linde P and Camanho P 2014 Micro-mechanical analysis of the in situ effect in polymer composite laminates, *Comp. Struct*, **116**, 827–840
[16] Farkas L, Vanclooster K, Erdelyi H, Sevenois R D B, Lomov S V, Naito T, Urushiyama Y and and Van Paepegem W 2016 Virtual material characterization process for composite materials: an industrial solution," in *Proc. of the 17th European. Conf. on Composite Materials* ,26–30, *Munich*
[17] Catera P G, Gagliardi F, Mundo D, De Napoli L, Matveeva A and Farkas L 2017 Multi-scale modeling of triaxial braided composites for FE-based modal analysis of hybrid metal-composite gears," *Comp. Struct.*, **182**, 116–123
[18] Matveeva A, Tabatabaei A, Sevenois R D B, Farkas L, Van Paepegem W and Lomov S V 2017 Assessement of different meso-modelling techniques for 2D woven composites, *in Proc* of the *NAFEMS conf : Multiscale and Multiphysics Modeling & Simulation - Innovation Enabling Technologies, At Columbus, OH,* USA
[19] Shishkina O, Matveeva A, Wiedemann S., Hoehne K, Wevers M, Lomov S V, Farkas L 2018 X-Ray Computed Tomograhy-based FE-Homogenization of sheared organo sheets, in *Proc. of the 18th European Conf. on Composite Materials, Athens, Greece*
[20] Melro A, Camanho P and Pinho S 2008 Generation of random distribution of fibres in long-fibre reinforced composites, *Comp. Science and Technology, **68**,* 2092–2102
[21] Romanov V, Lomov S V, Swolfs Y, Orlova S, Gorbatikh L and Verpoest I 2013 Statistical analysis of real and simulated fibre arrangements in unidirectional composites, *Composites Science and Technology*, **87**, 126–134
[22] X. Morelle 2015 Mechanical characterization and physics-based modeling of highly-crosslinked epoxy resin, PhD Thesis, UCL-Université Catholique de Louvain, Belgium
[23] Garoz D, Gilabert F A, Sevenois R D B, Spronk S. W. F and Van Paepegem W 2018 Consistent Application of Periodic Boundary Conditions in Implicit and Explicit Finite Element Simulations of Damage, t*o be submitted*
[24] Kassem G. A. 2009 Micromechanical material models for polymer composites through advanced numerical simulation techniques, *PhD Thesis*, RWTH Aachen University